Efficient radiative cooling coating with biomimetic human skin wrinkle structure

Ziming Cheng[1, 2, 4]†, Han Han[1, 2]†, Fuqiang Wang[2, 3]*, Yuying Yan[4], Xuhang Shi[1, 2], Huaxu Liang[1, 2], Xinping Zhang[1, 2], Yong Shuai[1, 3]

[1] School of Energy Science and Engineering, Harbin Institute of Technology, 92, West Dazhi Street Harbin 150001, P. R. China

[2] School of New Energy, Harbin Institute of Technology at Weihai, 2, West Wenhua Road, Weihai 264209, P. R. China

[3] Key Laboratory of Aerospace Thermophysics, Ministry of Industry and Information Technology, Harbin 150001, P. R. China

[4] Faculty of Engineering, University of Nottingham, Nottingham NG7 2RD, UK

†These authors contributed equally to this work.

*Corresponding author. Email: wangfuqiang@hitwh.edu.cn

Abstract: Daytime radiative cooling is an energy-free pathway to achieve cooling performance. Current radiative cooling materials with periodic photonic structures are facing a huge challenge in terms of scale expansion owing to complex preparation technology and high cost. Herein, we proposed the idea of the biomimetic wrinkle structure combined with optimized particles to achieve the efficient optical property regulation of both the solar band and "atmospheric window" band. On this basis, a large-scale radiative cooling coating with the biomimetic structure of human skin natural wrinkle, comprising high concentrations of $BaSO_4$ and SiO_2 particles, was demonstrated. The coating with a thickness of ~100 μm reflected ~95% of solar irradiance, and the emissivity in the "atmospheric window" band was ~96%. At noontime (11:00-13:00), in a populous area located at sea level, the average effective cooling power of ~89.6 W/m^2 was recorded, and the maximum sub-ambient temperature drop was 8.1 °C. An outdoor-building test conducted over a year showed that the maximum average indoor air temperature of the building painted with the coating was reduced by 6.2 °C and the maximum power-saving rate of air-conditioning exceeded 50%. Our work provided a new idea for designing, fabrication, and application of high-performance radiative cooling materials.

Keywords: radiative cooling; skin; biomimetic; natural wrinkles.

1. Introduction

With the progress of human civilization and rapid economic development, research has been focused on ensuring a comfortable living environment to meet the increasing demand for cooling [1-5]. However, the current cooling methods not only consume a lot of energy but also cause serious damage to the environment [6]. As an emerging and environment-friendly cooling technology, passive daytime radiative cooling (RC) can strongly reflect the solar irradiance (λ= 0.3–2.5 μm) and radiate infrared heat to outer space (3K) through the "atmospheric window" (λ= ~8–13 μm), thus inducing a sub-ambient temperature drop [7-10]. In future, RC materials can be widely used in zero-energy buildings, efficient solar cells, refrigerated trucks, and other related fields [11-16].

In recent years, inspired by the extremely skillful surface structures of silver antes and longicorn beetles, several high-performance photonic radiators with periodic nano/microstructures, including triangular prism array, pillar arrays, and pyramid structures, have been demonstrated using etching technology [17-21]. Cooling paints and polymers, with advantages of high expansibility, easy applicability, and inexpensiveness, have always been the benchmark for RC materials [22-24]. In addition, the optical properties of the currently reported particle-containing coatings still have much room for improvement [25-29]. In this study, we realized that the combination of surface structures and coatings was a feasible approach to design a coating type with high-performance RC coating. However, RC materials with surface structures were facing a huge challenge in terms of scale expansion due to the complex preparation technology, high cost, and low efficiency [30].

In addition to the RC material with the conventional periodic photonic structures, those with more commonly encountered natural wrinkles may perform equally well. Natural wrinkles, such as the wrinkles in human skin and orange, were usually caused by surface contraction or expansion. The main reason for the mechanical mechanism was that when the stress in the surface exceeded the critical value during solvent evaporation, it caused surface instability and triggers the formation of wrinkles [31]. The skin surface (Figs. 1(A), (B) and (C)) was naturally wrinkled at an average roughness of ~5 μm based on the flow rate of water and collagen. The average emissivity of the human body in the 8–13 μm band can reach 91.5%, as shown in Fig. 1(D). When the human body was at normal temperature and in a relaxed state, approximately 60% of the heat was lost through radiative heat transfer, and the skin played an important role as the emission surface [32]. As such, the coating form irregular wrinkles (at hardly additional cost) from the stress contraction because

of solvent volatilization during the drying process. We pondered whether the optical properties of the RC coating can be enhanced by the wrinkled surface structure. Accordingly, we demonstrated and tested an efficient biomimetic RC coating (Bio-RC coating) with natural wrinkles containing $BaSO_4$ and SiO_2 particles, as shown in Fig. 1(E) and (F). Specifically, we achieved a substrate-independent hemispherical reflectivity ($\overline{R}_{solar}$) of ~95% and an emissivity ($\overline{\varepsilon}_{atm}$) of ~96% with Bio-RC coating. These values demonstrated the significant performance of the proposed coating, for example, under a total solar irradiance of 803 W/m^2, the maximum sub-ambient temperature drops by ~8.1 °C and the average effective radiative cooling power was ~89.6 W/m^2. This cooling performance was on par with or exceeded those in reported previous studies [30, 33-36]. Compared with ordinary buildings, the maximum average indoor air temperature of the building painted with the Bio-RC coating was reduced by 6.2 °C, and the air-conditioning power-saving rate exceeded 50%. Furthermore, the coating demonstrated excellent substrate adaptability, color extensibility, and weatherability and was thus suitable for large-scale commercial applications.

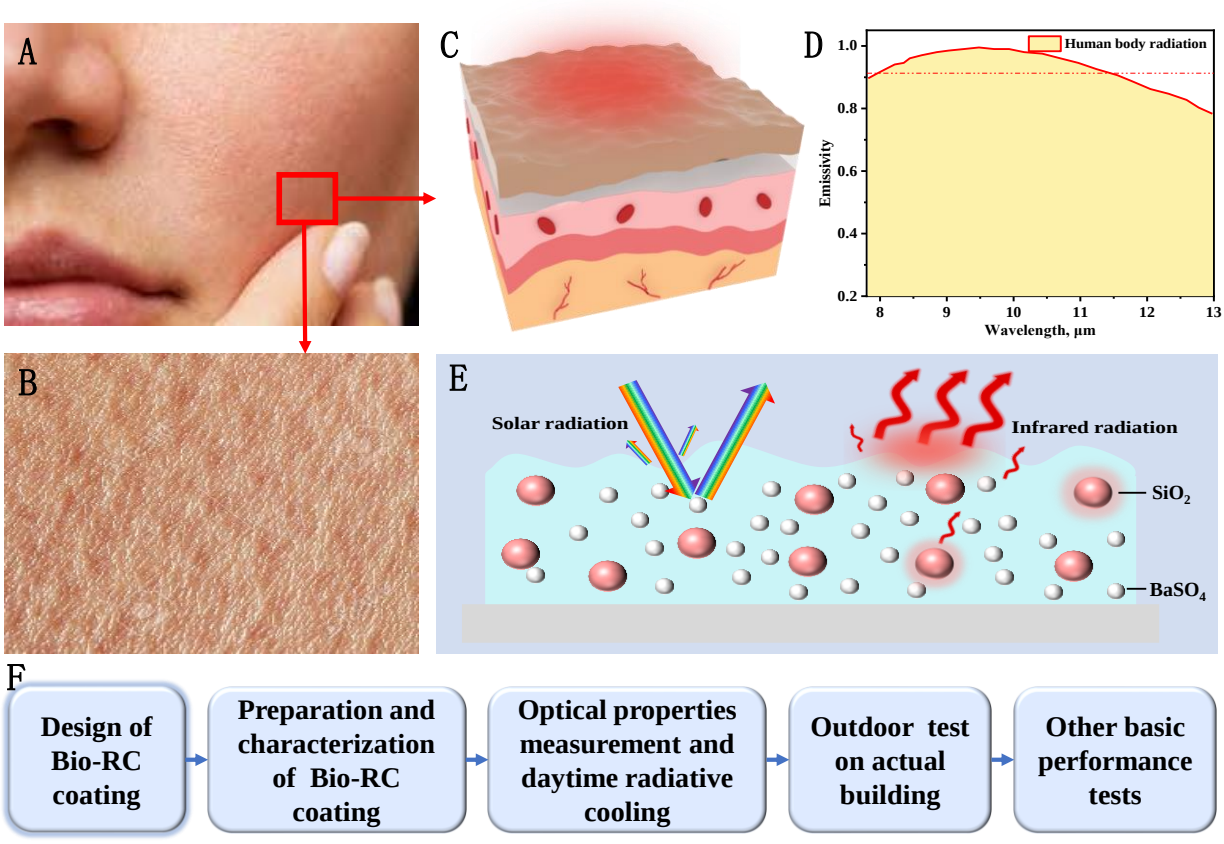

Fig. 1 Skin (A) Photos of human facial skin. **(B)** Locally enlarged view of the skin. **(C)** Schematic of the skin structure. **(D)** The emissivity of the human body at 8-13 μm. The dotted line in *D*

indicated average emissivity of 91.5%. **(E)** Basic working principle and schematic of the Bio-RC coating. **(F)** Flow chart of the Bio-RC coating.

2. Design of the Bio-RC coating

This study was aimed at producing a coating with improved optical propertied because of its wrinkled structure and added particles. As such, we used the finite difference time domain (FDTD) simulation to optimize related parameters. First, we optimized the size distributions of $BaSO_4$ and SiO_2 particles. As corroborated through FDTD simulation, SiO_2 particles with the size of 4 μm can effectively enhance the emissivity of the coating at 8–13 μm because smaller microsphere resonated at the electric dipolar resonance, while higher order electric and magnetic modes were excited in the larger microsphere (Fig. S5(A)) [25]. Moreover, $BaSO_4$ particles with the size of 0.4 μm, comparable with the wavelength of the incident light, generated strong Mie scattering, leading to enhanced reflectivity at the solar band (Fig. S5(B)) [37]. The variation in energy distribution with coating thickness was analyzed, and it was found that the thickness of the coating tended to be stable and reached 100 μm (Fig. S5(C)). Furthermore, the influence of different heights of wrinkle structure on the emissivity in the "atmospheric window" was analyzed, using the control variable method. The spectral and the average emissivity in the "atmospheric window" band of Bio-RC coatings with different heights of wrinkle structures were given (Fig. S6 (B) (C)), which showed that with the increase of the wrinkle height, the emissivity of the coating in the wavelength range of 8.0–13.0 μm significantly increased at first, then gradually decreased, and reached the maximum when the average height of wrinkles was 5 μm.

In the solar band, the average reflectivity ($\overline{R}_{solar}$) of the coating with wrinkled structure was 1.3% higher than that of the planar coating, and the average reflectivity ($\overline{R}_{solar}$) of the two coatings was 94.7% and 93.4%, respectively, as shown in Fig. 2(A). This was mainly due to the improvement of reflectivity in NIR wavelengths (λ= 0.78-2.5 μm) caused by Mie scattering (Fig. 2(B)). In the "atmospheric window" band, when the incident light was at the wavelength of 9.6 μm, the coating with the wrinkled structure absorbed the incident light energy within a short distance (Figs. 2(C) and (D)). The average emissivity ($\overline{\varepsilon}_{atm}$) was 4.5% higher with the wrinkled structure (96.2%) compared to 91.7% of the planar coating (Fig. 2(E)). This enhanced emissivity was because of the similar heights of the wrinkle and incident wavelength; as such, the photons cannot pass directly through the surface of the wrinkled structure and thus continue to oscillate

between the wrinkled structures. Therefore, the propagation path of photons increased, improving the emissivity. Moreover, the wrinkle destroyed the continuity of the surface, causing the fading wave to decay rapidly on the surface, which further improved the emissivity of the coating. The influence of the incident light at different angles on the spectral emissivity of the coating was calculated (Fig. 2(F)). As shown, the difference in the spectral emissivity between the coating with wrinkled structure and planar coating was the largest when the incident light was in the vertical direction (0°).

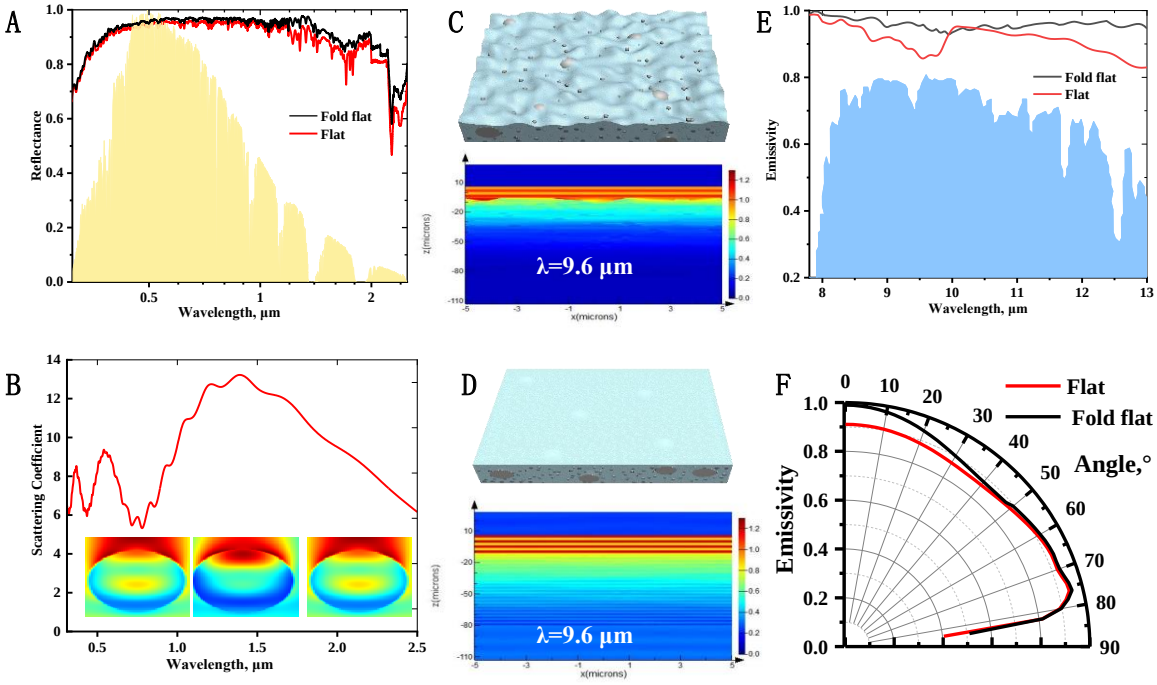

Fig. 2 Comparison of optical properties of the Bio-RC coating and planar RC coating (A) Comparison of solar reflectivity. **(B)** Scattering coefficient of the Bio-RC coating, inset picture was the electromagnetic field in light travels between single particles. Inset: Cross-sectional view of two-dimensional distribution of light intensity (square of the absolute value of the electric field component of light, or Electric field) for $BaSO_4$ particle **(C)(D)** Schematic of the Bio-RC and planar RC coatings; electromagnetic field distribution at 9.6 μm. **(E)** Comparison of emissivity. **(F)** Comparison of emissivity in "atmospheric window" at different incident angles.

3. Preparation and characterization of the Bio-RC coating

According to the abovementioned numerical analysis, the optimized Bio-RC coating had a wrinkled structure with an average height of 5.0 μm caused by evaporation of the solvent, in which

$BaSO_4$ and SiO_2 particles were randomly distributed (Fig. S5). The Bio-RC coating was fabricated using a simple roller coating method that included the following fabrication steps: ball-milling, weighing, ultrasonic oscillating, stirring, and drying (Fig. 3(A)). Polyvinylidene difluoride can be replaced with commonly used water-based substrates, such as acrylic and organosilicon resins. The scalability of our fabrication procedure and materials rendered the optimized Bio-RC coating promising for practical applications requiring large-area coatings.

The Bio-RC coating on the copper plate had a fairly whitish appearance (Fig. 3(B)). The scanning electron microscopic (SEM) image showed that the Bio-RC coating with ~100-μm thickness was tightly attached to the surface of the substrate. Owing to high filler concentration, the embedded particles were wrapped in the fabricated coating, showing a state of aggregation. The size distributions of $BaSO_4$ particles and SiO_2 particles were characterized by a laser light particle size analyzer, and the average diameters were 0.4 and 4.0 μm, respectively (Fig. 3(C)). The surface of the Bio-RC coating was observed using an optical microscope, which showed the formation of surface protrusions of a certain size due to the evaporation of the solvent during the drying process (Fig. 3(D)). To obtain clearer surface morphology of the Bio-RC coating, the 3D mode of the optical microscope was used to scan the surface of the coating with natural wrinkles (Fig. 3(E)), and the surface measurement results showed that the average roughness of the surface protrusions was ~5.0 μm.

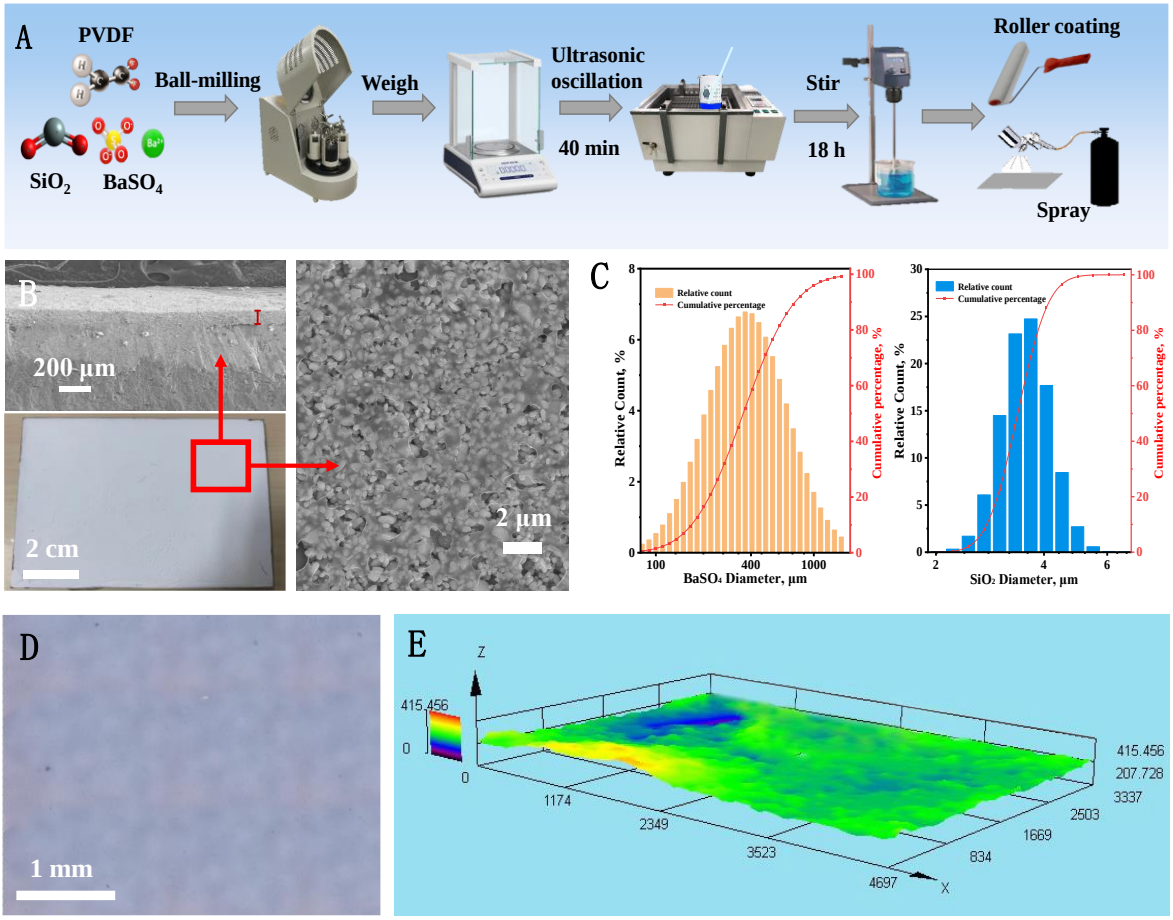

Fig. 3 Preparation and characterization of the Bio-RC coating (A) Preparation of the Bio-RC coating. **(B)** Lower left: Image of the Bio-RC coating; Upper left: SEM sectional diagram and Right: SEM image of the Bio-RC coating. **(C)** Size distributions of $BaSO_4$ and SiO_2 particles in Bio-RC coating, showing average diameter sizes of ~0.4 and ~4.0 μm, respectively. **(D)** Image of surface morphology of radiative cooling coating taken by optical microscope. **(E)** Image of coating surface in the 3D scanning mode of the optical microscope.

4. Results and discussion

4.1 Optical properties and daytime RC performance of the Bio-RC coating

The RC performance of the coating was mainly determined by its spectral properties in the solar and infrared bands. The spectral reflectance of the Bio-RC coating and planar coating was determined by UV-VIS-NIR spectrophotometer (0.3-2.5 μm) and Fourier infrared spectrometer (2.5-15.0 μm). For 100-μm-thick Bio-RC coating, the average reflectivity ($\overline{R}_{solar}$) in the solar spectrum was ~95%, and the average emissivity ($\overline{\varepsilon}_{atm}$) in the "atmospheric window" band was

~96%. Compared with the planar coatings of the same thickness, the wrinkled structure effectively increased the reflectivity in the solar spectrum by 1% and the emissivity by ~3%. (Fig. 4(C)).

The actual RC capability of the Bio-RC coating was tested in the densely populated city of Weihai, China (37°31′46″N, 122°4′40″E, sea level) on October 25th, employing the self-made experimental apparatus. To reduce the influence of heat convection and conduction on the accuracy of experimental results, polystyrene foam was covered with a high-reflective aluminum foil with super thermal insulation performance, and four short sticks were used to support the Bio-RC coating in the polystyrene foam. The Bio-RC coating painted on a 1-mm-thick copper sheet was subjected to direct sunlight under a clear sky (Figs. 4(A) and(B)). Temperatures of both the environment (air) and the Bio-RC coating were registered during the hottest period of the day (10:00–14:00), and the temperature variation curves for these were plotted in Fig. 4(D). The corresponding sub-ambient temperature drop (ΔT) (Fig. 4(E)) can be obtained by subtracting the two temperature curves. Interestingly, under an average total solar irradiance of I_{solar} = ~803 W/m^2 (Fig. 4(F)), average ambient temperature of ~27.9 °C, and average relative humidity of ~26.1% (Fig. 4(G)), the Bio-RC coating achieved the maximum temperature drop of ~8.1 °C and average temperature drop (ΔT) of ~5.9 °C. The cooling power of the Bio-RC coating was measured experimentally by using a self-built ingenious automatic feedback device. The temperature feedback control module controlled the heating film. The temperature of the copper plate was consistent with the ambient temperature, and the heating power was equivalent to the cooling power. The average effective cooling power was ~85.3 W/m^2 under the same experimental conditions (10:00-14:00) (Fig. 4(H)). Thereinto, the average effective cooling power of ~89.6 W/m^2 was recorded at noontime (11:00-13:00).

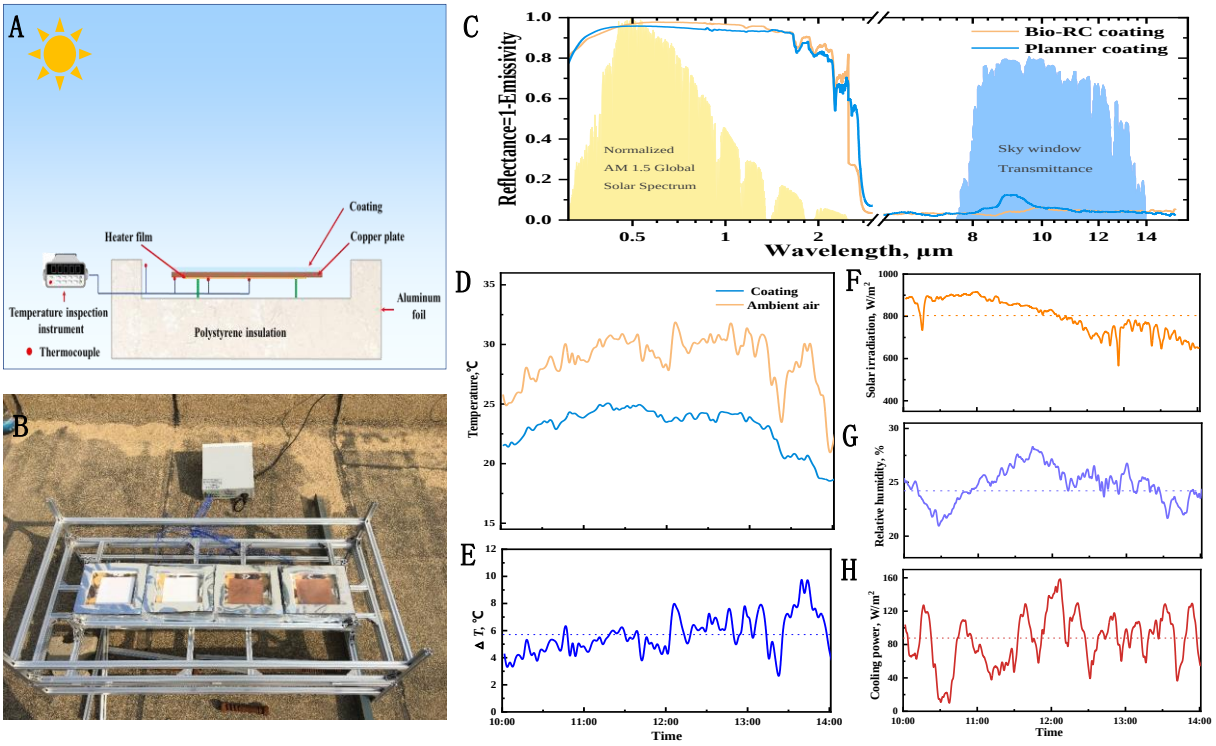

Fig. 4 Optical properties and daytime radiative cooling (RC) performance of the Bio-RC coating. (A) Schematic of a single testing device. **(B)** Photograph of the control experiment device for daytime RC performance. **(C)** The experimental reflectivity (1-emissivity) of the Bio-RC coating and planar coating in normalized ASTM G173 global solar spectrum and "atmospheric window" spectrum. **(D)** Temporal temperature data of air and Bio-RC coating under direct sunlight and **(E)** sub-ambient temperature drop (ΔT) of the Bio-RC coating. The dotted line in E indicated average ΔT of 5.1 °C. **(F–H)** Detailed average total solar irradiance, I_{solar} **(F)**; relative humidity **(G)**; and RC power **(H)** measured in the experiment; the average values of each curve in F–H were 803 W/m^2, 26.1%, and 85.3 W/m^2, respectively, shown as a dotted line in the corresponding graphs.

4.2 Outdoor test of the Bio-RC coating on the actual building

During applications, RC materials can be widely applied in many fields, particularly in outdoor buildings. To test the cooling performance of the Bio-RC coating in the actual building, we built two identical outdoor buildings on the open roof for comparative experiments; one was coated with the Bio-RC coating (Fig. 5*A*), while the other was coated with common blue paint. The temperature of the two roof surfaces was captured by an infrared thermal imager at noon on August 17th, 2020. Obtained from data of the infrared thermal images, the average roof temperature

of the building with/without the Bio-RC coating was 60.2/40.3 °C (Figs. 5 (B) and (C)); the temperature difference was up to 19.9 °C. In addition, the temperature data of the two buildings for three consecutive days (6.14–6.16, 2020) were measured using thermocouples (Fig 5(D)). The difference between the maximum roof temperatures of the two buildings was 23.6 °C, and the corresponding difference between the maximum indoor air temperatures was 13.9 °C. In the afternoon, the indoor air temperature increased owing to the solar radiation irradiating the wall; this affected the cooling performance of the Bio-RC coating, and this phenomenon would be greatly reduced in the application scene of a large area of the coating.

Furthermore, we constantly observed the actual cooling performance of the coating throughout the year (2019.10–2020.10) and compared the changes in roof surface and indoor air temperatures. As shown in Figs. 5(E) and 5(F), the temperature of the coated roof was significantly lower than that of the uncoated roof. Owing to the low ambient temperature and high wind speed in winter, the roof temperature difference in January was only 4.5 °C. Comparatively, in July, the roof temperature difference was the largest, reaching 11.3 °C. Owing to the existence of the roof insulation layer, the difference in the indoor air temperature was significantly smaller than that of the roof temperature. The indoor temperature difference in January was the least at 0.3 °C, whereas the difference in May was the largest at 6.2 °C.

The power-saving rate was another important indicator to evaluate the cooling performance of the Bio-RC coating; therefore, we conducted a 4-day (7.29–8.01, 2020) uninterrupted comparison experiment to obtain the power-saving performance. According to the notice of the General Office of the State Council on "Strictly implementing the air-conditioning temperature control standard in public buildings" in 2007, the indoor air-conditioning temperature setting in summer should not be lower than 26 ℃ for all public buildings [38, 39]. Therefore, during testing, the air-conditioning temperatures of the two rooms were set to 26 °C. The results showed that the power consumption of the air-conditioning in the coated room was significantly lower than that in the uncoated room, and the daily power-saving rates during testing were 23.5%, 23.8%, 26.9%, and 22.7%, respectively (Fig 5(G)). Take July 31 as an example, in three time periods of 7:00–10:00, 10:00–15:00, and 15:00–19:00, the power consumptions of the building with the Bio-RC coating were 0.4, 0.7, and 0.4 kWh, whereas the air-conditioning power consumptions of the uncoated room were 0.6, 1.0, and 0.6 kWh. The power-saving rates ($\xi_c = \frac{e_a - e_b}{e_b} \times 100\%$) in these three periods were 50.0%, 42.8%, and 50.0%, respectively. By using Bio-RC coating in Weihai,

the energy consumption could be saved up to 40.9 kWh in summer and had risen by only to 9.9 kWh in winter, resulting in a net energy saving of 31.0 kWh. In dry and hot areas, the application of Bio-RC coating could result in a larger net energy saving.

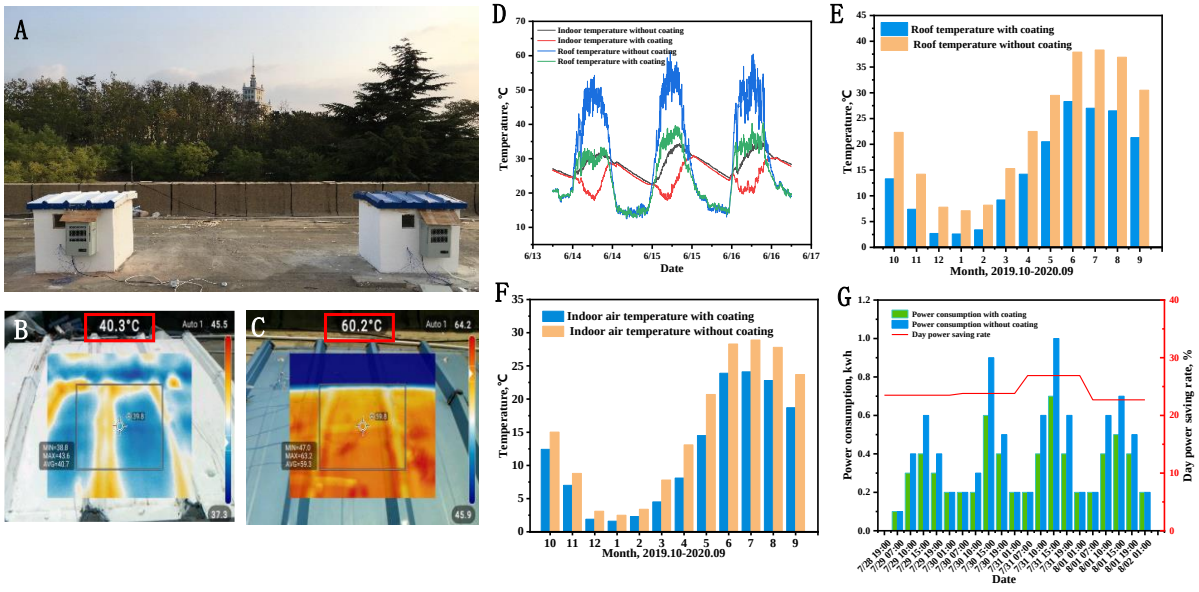

Fig. 5 Comparison of experimental results of buildings with/without Bio-RC coating. (A) Photograph of the two test buildings with air-conditioners; the roof of the left building was painted with the Bio-RC coating, while the right building was painted the ordinary paint. Further details were provided in the supplementary materials. Infrared thermal images of the building roof painted with the Bio-RC coating **(B)** and not painted with the Bio-RC coating **(C)**; Building continuous temperature test curve; the blue and black lines showed the uncoated-roof and indoor temperatures, respectively, and the green and red lines showed the coated-roof and indoor temperatures, respectively**(D)**. Comparative experimental result of the monthly average roof temperature **(E)** and indoor air temperature **(F)**; the blue column presented the temperature of the painted building, and the yellow column presented the temperature of the unpainted building. **(G)** The air-conditioning electricity consumption graph for each period (7:00–10:00, 10:00–15:00, 15:00–19:00, 19:00–01:00, and 01:00–07:00); the green column showed the coated power consumption, the blue column showed the uncoated power consumption, and the red line indicated the daily power saving rate.

4.3 Versatility of Bio-RC coating

The excellent optical performance of the Bio-RC coating was complemented by paint-like applicability, which was crucial for direct application on structures. The Bio-RC coating can be easily applied to different types of substrates such as stone, aluminum, plastic, and wood (Figs. 6 (A)–(D)). Furthermore, hardness was also a basic performance factor that affected the service life of the Bio-RC coating, and minor scratches appeared when a 3H pencil was traversed on the surface of the Bio-RC coating (Fig. S9).

Owing to practical requirements for color appearance in practical scenes, the color extensibility of RC coating was particularly important [40, 41]. Ordinary paints usually had low reflectance in the NIR wavelengths [42]. To minimize solar radiation, the colored coatings should maximize the reflection of NIR wavelengths. We added coloring to the paint prepared red, yellow, and blue Bio-RC coatings; and tested the spectral performances (Fig. 6(E)). The average reflectivity of the red, yellow, and blue Bio-RC coatings in the NIR wavelengths was ~94%, which was equivalent to the average reflectivity of the ordinary Bio-RC coating. Based on the analysis of the spectral data, the chromaticity of the blue, red, and yellow Bio-RC coatings was shown in the CIE 1931 color space (Fig. 6(F)).

Long-term outdoor exposure caused dust to contaminate the coating surface, thus affecting the cooling performance. To this end, we sprayed a layer of polytetrafluoroethylene on the surface of the Bio-RC coating to achieve a hydrophobic property hardly affecting the optical performance conditions. The Bio-RC coating had a high-water contact angle of ~125.3°, which had a potential self-cleaning function. To verify the durability of the coating, the spectral reflectivity of the Bio-RC coating that had been exposed outdoor for ten months (2020.10-2021.7) was measured. The optical properties of the Bio-RC coating were almost unchanged, proved the Bio-RC coating with a great durability (Fig. S10).

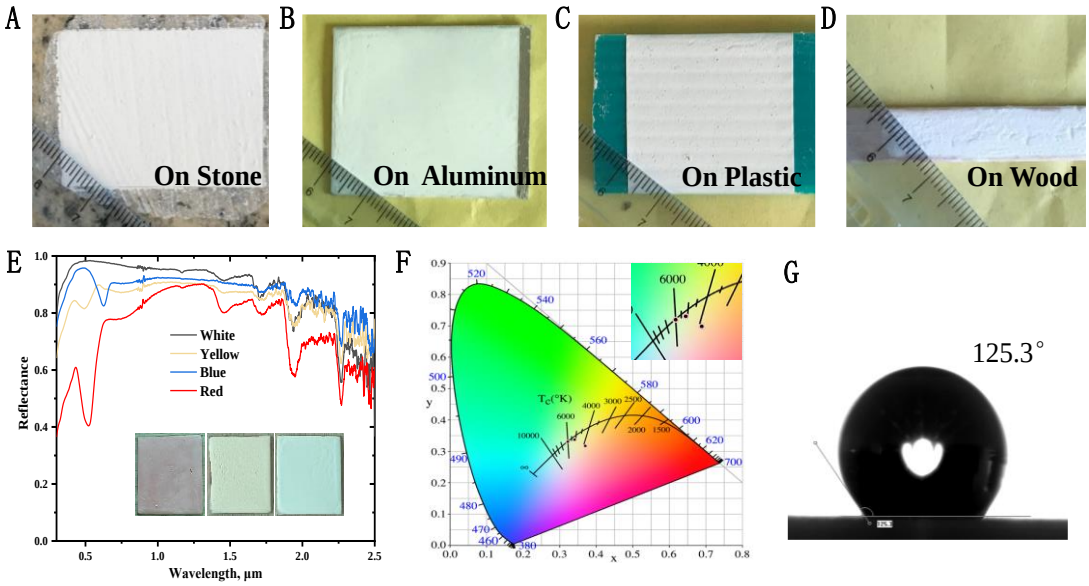

Fig. 6 Versatility of Bio-RC coatings. The Bio-RC coating can be **(A)** painted on stone, **(B)** painted on aluminum, **(C)** painted on plastic, or **(D)** dip-coated on wood. **(E)** The spectral reflectivity of yellow, red, and blue Bio-RC coating compared to that of a white Bio-RC coating; the insets showed three color samples. **(F)** The chromaticity of the red, yellow, and blue Bio-RC coting shown in the CIE 1931 color space; the inset presented the enlarged view of the chromaticity values of the coatings. **(G)** Photograph of the contact angle for the droplet (the average value was 125.3°).

5. Conclusions

In this paper, we proposed the idea of the biomimetic wrinkle structure combined with optimized particles to achieve the efficient optical property regulation of both solar band and "atmospheric window" band. On this basis, we demonstrated a radiative cooling coating with the biomimetic structure of human skin natural wrinkle, comprising high concentrations of $BaSO_4$ and SiO_2 particles. The Bio-RC coating with a thickness of ~100 μm can reflect ~95% of solar irradiance (0.3-2.5 μm), and the emissivity in the "atmospheric window" band (8.0-13.0 μm) was ~96%. At noon time, in a populous area located at sea level, the average cooling power of 85.3 W/m^2 was recorded, and the maximum sub-ambient temperature drop was 8.1 °C. An outdoor-building test conducted over a year showed that, compared with ordinary buildings, the maximum average indoor air temperature of the building painted with the Bio-RC coating was reduced by 6.2 °C, and the maximum power-saving rate of air-conditioning exceeded 50%. Furthermore, the coating exhibited excellent substrate adaptability, color extensibility, weather ability and at a cost

of only \$1.8/m^2 and was thus suitable for large-scale commercial applications. This work provided a new idea for designing, fabrication, and application of high-performance radiative cooling materials.

6. Materials and Methods

6.1 Preparation of the Bio-RC coating and planar coating

All chemicals were of analytical grade purity and used directly without further purification. Firstly, the $BaSO_4$ and SiO_2 particles were ground into 0.4 and 4.0 μm by using ball milling, respectively. Then, $BaSO_4$/SiO_2 particles were added to N-methyl pyrrolidone (NMP) for ultrasonic vibration dispersion for 30 min to achieve stable turbidity. The PVDF was gradually added to the turbidity while stirring; the mixture was then stabilized over 10 h. After stirring and stabilizing, the paint achieved applicable viscosity that it formed a stable and continuous wire drawing state when it was stained by the glass rod. When the Bio-RC coating can be conventionally sprayed or painted on the copper plate, the thickness of the coating should be slightly below the maximum thickness of the coating allowed by surface tension. Finally, the Bio-RC coating was obtained after drying in an oven at 70 °C for 20 min to make the adhesion stronger or naturally drying.

The planar coating was prepared using the same paint. The paint was applied to the surface of the smooth silver mirror and peeled off after drying, obtaining the planar coating.

6.2 Outdoor test device of actual building

Two identical outdoor test chambers of 0.9 m × 0.9 m × 1.2 m (length × width × height) were built. The top layer was a 2-mm-thick iron plate, with a 10-cm-thick insulating foam layer and wall thickness of 15 cm. There were 15 cm × 15 cm glass windows on the north wall of the air blocking brick (Fig. 5(A)). One building was coated with an RC coating on the top, and the other one was kept uncoated. A temperature measuring thermocouple was arranged on the top of the house to measure the surface temperature of the roof, and a temperature-measuring thermocouple was arranged inside the house to measure the indoor air temperature. The cabinet air conditioner was installed separately, and the electric energy meter was connected separately to measure the electricity consumption of the room at each time. The air-conditioner temperature was set to 26 °C for the power-saving test.

References

[1] K.T. Lin, J. Han, K. Li, C. Guo, H. Lin, B. Jia, Radiative cooling: Fundamental physics, atmospheric influences, materials and structural engineering, applications and beyond, Nano Energy 80 (2021) 105517.

[2] Q. Zeng, Y. Wu, Q Tang, W. Liu, J. Wu, Y. Zhang, G. Yin, H. Yang, S. Yuan, D, Tan, C. Hu, X. Wang, A high-efficient breeze energy harvester utilizing a full-packaged triboelectric nanogenerator based on flow-induced vibration. Nano Energy 70 (2020) 104524.

[3] T. Wang, Y. Wu, L. Shi, X. Hu, M. Chen, L. Wu, A structural polymer for highly efficient all-day passive radiative cooling, Nat. Commun. 12(1) (2021) 365.

[4] B. Zhao, M. Hu, X. Ao, N. Chen, G. Pei, Radiative cooling: A review of fundamentals, materials, applications, and prospects, Appl. Energy 236 (2019) 489-513.

[5] D. Han, B.F. Ng, M.P. Wan, Preliminary study of passive radiative cooling under Singapore's tropical climate, Sol. Energ. Mat. Sol. C. 206 (2020) 110270.

[6] Z. Xia, Z. Fang, Z. Zhang, K. Shi, Z. Meng, Easy Way to Achieve Self-Adaptive Cooling of Passive Radiative Materials, ACS Appl. Mater. Interfaces 12(24) (2020) 27241-27248.

[7] A.R. Gentle, G.B. Smith, Radiative heat pumping from the Earth using surface phonon resonant nanoparticles, Nano Lett. 10(2) (2010) 373-379.

[8] A.P. Raman, M.A. Anoma, L. Zhu, E. Rephaeli, S. Fan, Passive radiative cooling below ambient air temperature under direct sunlight, Nature 515(7528) (2014) 540-544.

[9] Z. Chen, L. Zhu, A. Raman, S. Fan, Radiative cooling to deep sub-freezing temperatures through a 24-h day-night cycle, Nat. Commun. 7 (2016) 13729.

[10] Z. Cheng, F. Wang, H. Wang, H. Liang, L. Ma, Effect of embedded polydisperse glass microspheres on radiative cooling of a coating. Int. J Therm Sci 140 (2019) 358-367.

[11] D. Zhao, A. Aili, Y. Zhai, J. Lu, D. Kidd, G. Tan, X. Yin, R. Yang, Subambient Cooling of Water: Toward Real-World Applications of Daytime Radiative Cooling, Joule 3(1) (2019) 111-123.

[12] J. Mandal, Y. Yang, N. Yu, A.P. Raman, Paints as a Scalable and Effective Radiative Cooling Technology for Buildings, Joule 4(7) (2020) 1350-1356.

[13] X. Xue, M. Qiu, Y. Li, Q. Zhang, S. Li, Z. Yang, C. Feng, W. Zhang, J. Dai, D. Lei, W. Jin, L. Xu, T. Zhang, J. Qin, H. Wang, S. Fan, Creating an Eco-Friendly Building Coating with Smart Subambient Radiative Cooling, Adv. Mater. 32(42) (2020) e1906751.

[14] M. Hu, B. Zhao, X. Ao, Suhendri, J. Cao, Q. Wang, S. Riffat, Y. Su, G. Pei, Performance analysis of a novel bifacial solar photothermic and radiative cooling module, Energy Convers. Manag. 236 (2021) 114057.

[15] S. Khan, J. Kim, K. Roh, G. Park, W. Kim, High power density of radiative-cooled compact thermoelectric generator based on body heat harvesting, Nano Energy 87 (2021) 106180.

[16] E. Mu, Z. Wu, Z. Wu, X. Chen, Y. Liu, X. Fu, Z. Hu, A novel self-powering ultrathin TEG device based on micro/nano emitter for radiative cooling, Nano Energy 55 (2019) 494-500.

[17] N.N. Shi, C.C. Tsai, F. Camino, G.D. Bernard, N. Yu, R. Wehner, Keeping cool: Enhanced optical reflection and radiative heat dissipation in Saharan silver ants, Science 349(6245) (2015) 298-301.

[18] P.C. Hsu, X. Li, Photon-engineered radiative cooling textiles, Science 370(6518) (2020) 784-785.

[19] S.Y. Jeong, C.Y. Tso, Y.M. Wong, C.Y.H. Chao, B. Huang, Daytime passive radiative cooling by ultra emissive bio-inspired polymeric surface, Sol. Energ. Mat. Sol. C.206 (2020) 110296.

[20] M. Yang, W. Zou, J. Guo, Z. Qian, H. Luo, S. Yang, N. Zhao, L. Pattelli, J. Xu, D.S. Wiersma, Bioinspired "Skin" with Cooperative Thermo-Optical Effect for Daytime Radiative Cooling, ACS Appl. Mater. Interfaces 12(22) (2020) 25286-25293.

[21] A. Krishna, X. Nie, A.D. Warren, J.E. Llorente-Bousquets, A.D. Briscoe, J. Lee, Infrared optical and thermal properties of microstructures in butterfly wings, Proc. Natl. Acad. Sci. 117(3) (2020) 1566-1572.

[22] Z. Cheng, F. Wang, D. Gong, H. Liang, Y. Shuai, Low-cost radiative cooling blade coating with ultrahigh visible light transmittance and emission within an “atmospheric window”, Sol. Energ. Mat. Sol. C. 213 (2020) 110563.

[23] W. Song, X. Wang, H. Qiu, N. Wang, M. Yu, Z. Fan, S. Ramakrishna, H. Hu, Y.Z. Long, Single electrode piezoelectric nanogenerator for intelligent passive daytime radiative cooling, Nano Energy 82 (2021) 105695.

[24] J. Fan, C. Fu, T. Fu, Yttria-stabilized zirconia coating for passive daytime radiative cooling in humid environment, Appl. Therm. Eng. 165 (2020) 114585.

[25] Y. Zhai, Y. Ma, S.N. David, D. Zhao, R. Lou, G. Tan, R. Yang, X. Yin, Scalable-manufactured randomized glass-polymer hybrid metamaterial for daytime radiative cooling, Science 355(6329) (2017) 1062-1066.

[26] G. Chen, Y. Wang, J. Qiu, J. Cao, Y. Zou, S. Wang, J. Ouyang, D. Jia, Y. Zhou, A visibly transparent radiative cooling film with self-cleaning function produced by solution processing, J. Mater. Sci. Technol. 90 (2021) 76-84.

[27] D. Li, X. Liu, W. Li, Z. Lin, B. Zhu, Z. Li, J. Li, B. Li, S. Fan, J. Xie, J. Zhu, Scalable and hierarchically designed polymer film as a selective thermal emitter for high-performance all-day radiative cooling, Nat. Nanotechnol. 16(2) (2021) 153-158.

[28] J. Mandal, Y. Fu, A.C. Overvig, M. Jia, K. Sun, N.N. Shi, H. Zhou, X. Xiao, N. Yu, Y. Yang, Hierarchically porous polymer coatings for highly efficient passive daytime radiative cooling, Science 362(6412) (2018) 315-319.

[29] Y. Peng, J. Chen, A.Y. Song, P.B. Catrysse, P.C. Hsu, L. Cai, B. Liu, Y. Zhu, G. Zhou, D.S. Wu, H.R. Lee, S. Fan, Y. Cui, Nanoporous polyethylene microfibres for large-scale radiative cooling fabric, Nat. Sustain. 1(2) (2018) 105-112.

[30] H. Zhang, K.C.S. Ly, X. Liu, Z. Chen, M. Yan, Z. Wu, X. Wang, Y. Zheng, H. Zhou, T. Fan,

Biologically inspired flexible photonic films for efficient passive radiative cooling, Proc. Natl. Acad. Sci.117(26) (2020) 14657-14666.
[31] Y. Tan, B. Hu, J. Song, Z. Chu, W. Wu, Bioinspired Multiscale Wrinkling Patterns on Curved Substrates: An Overview, Nano-Micro Letters, 12(1) (2020).
[32] P.C. Hsu, C. Liu, A.Y. Song, Z. Zhang, Y. Peng, J. Xie, K. Liu, C.-L. Wu, P.B. Catrysse, L. Cai, A dual-mode textile for human body radiative heating and cooling, Sci. Adv. 3(11) (2017) e1700895.
[33] H. Bao, C. Yan, B. Wang, X. Fang, C.Y. Zhao, X. Ruan, Double-layer nanoparticle-based coatings for efficient terrestrial radiative cooling, Sol. Energ. Mat. Sol. C. 168 (2017) 78-84.
[34] M. Chen, D. Pang, J. Mandal, X. Chen, H. Yan, Y. He, N. Yu, Y. Yang, Designing Mesoporous Photonic Structures for High-Performance Passive Daytime Radiative Cooling, Nano Lett. 21(3) (2021) 1412-1418.
[35] D. Fan, H. Sun, Q. Li, Thermal control properties of radiative cooling foil based on transparent fluorinated polyimide, Sol. Energ. Mat. Sol. C. 195 (2019) 250-257.
[36] B. Xiang, R. Zhang, Y. Luo, S. Zhang, L. Xu, H. Min, S. Tang, X. Meng, 3D porous polymer film with designed pore architecture and auto-deposited SiO2 for highly efficient passive radiative cooling, Nano Energy 81 (2021) 105600.
[37] Z. Cheng, Y. Shuai, D. Gong, F. Wang, H. Liang, G. Li, Optical properties and cooling performance analyses of single-layer radiative cooling coating with mixture of TiO_2 particles and SiO2 particles, Sci China Technol Sc 64(5) (2020) 1017-1029.
[38] http://www.gov.cn/gongbao/content/2007/content_678925.htm
[39] http://www.wasion.com/Art/1649.aspx
[40] S. Son, S. Jeon, D. Chae, S.Y. Lee, Y. Liu, H. Lim, S.J. Oh, H. Lee, Colored emitters with silica-embedded perovskite nanocrystals for efficient daytime radiative cooling, Nano Energy 79 (2021) 105461.
[41] Y. Chen, J. Mandal, W. Li, A. Smith-Washington, C.-C. Tsai, W. Huang, S. Shrestha, N. Yu, R.P.S. Han, A. Cao, Y. Yang, Colored and paintable bilayer coatings with high solar-infrared reflectance for efficient cooling, Sci. Adv. 6(17) (2020) eaaz5413.
[42] J. Song, J. Qin, J. Qu, Z. Song, W. Zhang, X. Xue, Y. Shi, T. Zhang, W. Ji, R. Zhang, The effects of particle size distribution on the optical properties of titanium dioxide rutile pigments and their applications in cool non-white coatings, Sol. Energ. Mat. Sol. C. 130 (2014) 42-50.

Acknowledgments:

This work was supported by National Key R&D Program of China grant (2018YFA0702300) and National Natural Science Foundation of China (52076064) and Taishan Scholars of Shandong Province grant (tsqn201812105) and EU ThermaSMART under (H2020-MSCA-RISE 778104)

and China Scholarship Council (202006120215). We also thank CSC grant for Ziming Cheng's scholarship of research visiting at University of Nottingham, UK.

Author contributions:

Ziming Cheng and Han Han conceived the concept and designed experiments. Ziming Cheng, Han Han and Xuhang Shi. contributed to experiments and data analysis. Han Han, Huaxu Laing and Xinping Zhang performed the simulations. Ziming Cheng and Fuqing Wang wrote the manuscript. Fuqiang Wang, Yong Shuai and Yuying Yan reviewed and edited the manuscript.

Competing interests:

Authors declare that they have no competing interests.

Data and materials availability:

All data are available in the main text or the supplementary materials. requests should be directed to the corresponding authors.

Appendix A. Supporting information

Supplementary Text

Figs. S1 to S10

Tables S1 to S2

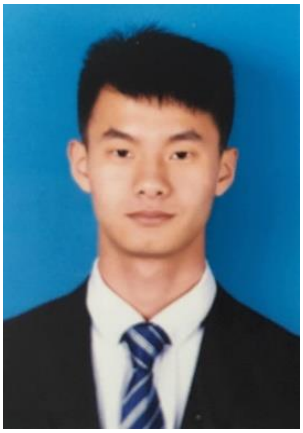

Ziming Cheng earned a B.S. degree in Energy and Power Engineering in 2016 from China University of Petroleum, and a M.E. degree in Power Engineering and Engineering Thermophysics in 2018 from Harbin Institute of Technology. He is now a Ph.D. candidate in Power Engineering and Engineering Thermophysics in Harbin Institute of Technology. Currently, his research work focuses on radiative cooling, efficient use of solar energy, solar spectrum regulation and large-scale fabrication.

Han Han earned a B.S degree in School of New Energy in 2020 from Harbin Institute of Technology at Weihai. Currently, He is obtaining his M.E. degree in Power Engineering and Engineering Thermophysics in Harbin Institute of Technology. He is working on radiative transfer and light-matter interaction. His research interests are mainly focusing on radiative cooling.

Fuqiang Wang is a full professor in the School of Energy Science and Engineering at Harbin Institute of Technology, and a full professor in the School of New Energy at Harbin Institute of Technology at Weihai. He received the B.S. degree in 2005 from China University of Petroleum. He received the Ph.D. degree in Power Engineering and Engineering Thermophysics in Harbin Institute of Technology in 2011. His current research interests are radiative cooling, solar spectral radiative transfer regulation, and energy-saving film related to thermal radiative transfer regulation fabrication.

Yuying Yan is Professor (Chair) in Thermofluids Engineering at the University of Nottingham, UK. He acted as Coordinator of UK-China international joint laboratory of Biomimetic Functional Surfaces and fluids. He received B.S. in Internal Combustion Engineering in 1982 at Jilin University of Technology, and received PhD in Mechanical Engineering in 1996 at City University of London, UK. His current research interests are cross-disciplinary subject of biomimetics, heat transfer, applied thermodynamics and so on.

Xuhang Shi earned a B.S. degree in College of Water Conservancy and Civil Engineering in 2019 from Shandong Agricultural University. He is now a Ph.D. candidate in Power Engineering and Engineering Thermophysics in Harbin Institute of Technology. Currently, his research work focuses on efficient use of solar energy, methane reforming hydrogen production in solar thermochemical porous media reactor.

Huaxu Liang earned a B.S. degree in School of Automotive Engineering in 2018 from Harbin Institute of Technology at Weihai. Currently, He is obtaining his Ph.D. in School of Energy Science and Engineering of Harbin Institute of Technology. He is working on full spectrum solar energy utilization, radiative transfer in nanofluid, and light control in the wave-optics regime. His research interests are mainly focusing on solar spectral radiative transfer regulation, spectral splitting based on optical film, and spectral splitting based on semitransparent PV.

25

Xinping Zhang is currently pursuing the M.E. degree in Power Engineering and Engineering Thermophysics at Harbin Institute of Technology at Weihai, China. His current research interest includes efficient use of solar energy, radiative transfer, and radiative cooling.

Yong Shuai is a full professor in the School of Energy Science and Engineering at Harbin Institute of Technology, China. He received the B.S. degree in 2001 and Ph.D. degree in 2006, from Harbin Institute of Technology, both in Power Engineering and Engineering Thermophysics. His current research interests are optical thermal regulation via Metamaterial and device fabrication and measurement of optical/thermal properties of materials.